I-V characteristics in two-dimensional frustrated Josephson-junction arrays

F. Falo,* A. R. Bishop, and P. S. Lomdahl
Theoretical Division and Advanced Studies Program, Los Alamos National Laboratory, Los Alamos, New Mexico 87545
(Received 16 November 1989)

Langevin molecular-dynamics simulations of two-dimensional Josephson-junction arrays in a uniform external magnetic field are presented. I-V characteristics for zero and finite temperature are calculated. The voltage response is analyzed in terms of the dynamical behavior of defects with respect to the ground-state flux lattice—domain walls and vortex-antivortex pairs. At zero temperature, several spatio-temporal regimes as a function of I are found: (i) a superconducting phase ($V=0$) corresponding to the locking of the flux lattice; (ii) a "chaotic" response related to domain walls nearly pinned by the discreteness of the underlying flux lattice; and (iii) two phases with ac response corresponding to different periodic domain-wall lattice patterns. At finite temperatures the response is modified by the nucleation of transverse structure (vortex-antivortex pairs) on the moving domain walls. This instability can enhance or inhibit the voltage response depending on the domain-wall structure. A phase diagram of the different dynamical regimes is proposed.

I. INTRODUCTION

Considerable attention has been devoted in recent years to studying of the properties of two-dimensional (2D) Josephson junctions arrays (JJA's).[1-7] Such studies have importance in their own right since modern lithographic techniques allow the construction of arrays of many geometries so that theoretical predictions can be tested experimentally. On the other hand, JJA's are the discrete version of a 2D superconductor assuming the lattice spacing to be of the order of the coherence length. In this framework a complete translation between JJA and 2D superconductor languages exists.[8] Also granular superconductors have been modeled by arrays of weak links. High-T_c superconductors belong to this last category because of their ceramic structure—due to the short coherence length of these materials, structural imperfections such as twin boundaries also weaken the superconductivity. It has been suggested that a hierarchy of weak links of different length scales may provide a model on which to base a "glassy" macroscopic phenomenology for these materials.[8]

Most of the information already available on 2D JJA's concerns *static* properties. In the *absence* of any external magnetic field, the 2D JJA is equivalent to the classical 2D XY magnet.[5] For example, the resistivity transition can be explained in terms of a Kosterlitz-Thouless[9,10] transition: i.e., vortex-antivortex pairs are thermally excited and unbind at T_c giving a finite resistivity in the JJA case. In the presence of a perpendicular magnetic field, the system is equivalent to a uniformly *frustrated* XY magnet. The ground state can be described by using a flux lattice language.[5] For *rational* values ($f=p/q$, where p and q have noncommon divisors) of the magnetic field (measured in units of flux quanta) two species of flux with values $(-f)$ and $(1-f)$ form a $q\times q$ periodic square flux lattice. Two kinds of excitations are possible in these ground states: one is the interchange of two different kinds of flux (which correspond to a vortex-antivortex excitations in the pure XY model) and the other is a domain wall that breaks the discrete symmetry of the flux lattice. Both excitations play an important role in the properties of the phase transitions for the frustrated model. For *irrational* values of the magnetic field, nonperiodic flux lattices with spin-glass-like behavior have been found: these are characterized by defects occurring with respect to a neighboring periodic (locked) flux lattice.[4]

An equivalent flux lattice representation is in terms of a Coulomb gas of excess positive charges with respect to a neutral $f=0$ background. Then the excess positive charges $(+1)$ have to be defined on the underlying square lattice, but are driven by logarithmic Coulomb interactions towards a hexagonal lattice structure (as for flux lattices in superconductors). This *competition* of length scales is the source of complexity discussed in this paper. As temperature increases, vortex-antivortex excitations can appear in the neutral background screening the Coulomb interactions and leading to melting of the lattice of positive charges and/or the neutral background (i.e., unbinding of vortex-antivortex pairs).

The dynamics of a 2D JJA is much less well studied[1,2,6] than the statics but provides an excellent controlled laboratory example with which to probe pattern formation and complex dynamics in competing interacting systems. Such systems are appreciated increasingly in many condensed matter and materials contexts[11]—e.g., the I-V characteristics of superconductors (above). The dynamics of a JJA (without magnetic field) can be derived from the dynamical theory of the Kosterlitz-Thouless transition.[2,10] At $T=0$ the array behaves like a single Josephson junction. At finite temperature, voltage response to a driving current is expected to have the nonlinear behavior $V\approx I^{1+a(T)}$, coming from the field-induced unbinding of vortex-antivortex dipoles. This scaling form is consistent with molecular dynamics simulations.[1] However, in the case of frustrated arrays the role of domain walls in the dynamics is not well understood, and gives deviations from the simple predictions.

In this paper, we study the dynamics of frustrated JJA's using a Langevin molecular dynamics technique with overdamped dynamics. Our main results are concerned with the study of the dynamics of a JJA in a perpendicular magnetic field which we set to achieve $\frac{1}{3}$ of quantum flux per plaquette (i.e., $f=\frac{1}{3}$). With this value, the ground state is highly degenerate and anisotropic, so we can expect a rich variety of domain-wall excitations. At zero temperature and with a spatially uniform driving current only extended defects (i.e., domain walls) can be excited. Due to the pinning effect of the lattice discreteness the ground-state flux lattice "melts" by the field nucleation of a one-dimensional domain-wall lattice. Depending on the strength of the driving current, very different patterns of the flux lattice are found and correlated with interesting dynamical behaviors. In particular, ac voltages are driven by dc currents. This ac effect is understood by the formation of solitonlike defects in the flux lattice. A dynamical transition between metastable configurations is also observed, as well as a "chaotic" ("noisy") regime near the flux flow threshold. The driven JJA is indeed seen to provide fascinating examples of space-time complexity and pattern formation.

At finite temperatures, local inhomogenous defects are thermally excited (vortex-antivortex pairs) in addition to domain walls. Both of these excitations determine the nature of the I-V characteristics for low currents. We observe how these local excitations provide the mechanism for the domain-wall motion at low currents and decrease the critical current at finite temperatures. A scenario for the critical behavior is discussed in the following. To briefly summarize, we find evidence for the following: (a) discrete lattice pinning of domain walls in the flux lattice background potential; (b) "chaotic" dynamics associated with motion of domain walls in a potential that varies according to individual local environments of lattice discreteness and domain walls; (c) transverse instabilities on moving domain walls nucleated thermally as vortex-antivortex pairs; (d) two characteristic temperatures corresponding to domain-wall melting and vortex-antivortex unbinding; and (e) critical driving currents corresponding to transitions of patterns in moving domain-wall lattices. This rich variety of phenomena leads to distinct regions in the temperature-driving current parameter space dominated by either thermal or field nucleation.

This paper is organized as follows. First, in Sec. II, the model used and the equation of motion for Langevin molecular dynamics (MD) are derived. Section III reports the main results at zero and finite temperature and discusses them. Finally, in Sec. IV, the conclusions of this work and future research directions are discussed.

II. MODEL AND SIMULATIONS

Consider a 2D square array ($L\times L=N$) of superconducting islands with weak links lying on the bonds. The Josephson energy for this 2D array in the presence of a perpendicular static magnetic field is given by

$$E_P=-E_j\sum_{\langle i,j\rangle}\cos(\theta_i-\theta_j-A_{ij})\ , \tag{1}$$

where $E_j=(\hbar/2e)I_c$ is the Josephson coupling, θ_i is the order-parameter phase in each superconducting island i with coordinates (i_x,i_y) and A_{ij} are lying along the links so that

$$\sum_{\text{plaquette}}A_{ij}=2\pi\frac{\Phi}{\Phi_0}=2\pi f\ . \tag{2}$$

Here Φ is the flux of the external magnetic field through the plaquette and $\Phi_0=hc/2e$ is the flux quantum. The parameter f fixes the "degree" of frustration of the phase lattice. For $f=0$ and $f=\frac{1}{2}$, Eq. (1) reduces, respectively, to the unfrustrated and fully frustrated XY models, both of which have been extensively studied in the past fifteen years (at least regarding their static properties).[3-5,9,12] We have chosen the A_{ij} in such a way that they equal $2\pi f\ i_y$ on the horizontal bonds and zero on the vertical ones, i.e., the Landau gauge.

We can introduce the *dynamics* in our problem by using a resistance-capacitance shunted junction model (RSJ). We start by considering the most general case in which we have an arbitrary capacitance matrix, C_{ij}. Then the energy associated with charge distribution in the lattice is

$$E_K=\frac{1}{2\alpha}\sum_{i,j}\dot\theta_i C_{ij}\dot\theta_j=\tfrac{1}{2}\alpha\sum_{i,j}p_i C_{ij}^{-1}p_j\ , \tag{3}$$

where $\alpha=4e^2/\hbar^2$ and we have defined

$$p_i=dE_K/d\dot\theta=(1/\alpha)\sum_k C_{ki}\dot\theta_k\ .$$

At this point we can construct the Hamiltonian $H_0=E_K+E_p$ and write the equations of motion for the variables p_i and θ_i. These equations read

$$\begin{aligned}\dot\theta_i&=\alpha\sum_s C_{is}^{-1}p_s\ ,\\ \dot p_i&=E_J\sum_\delta\sin(\theta_{i+\delta}-\theta_i-A_{i,i+\delta})\ ,\end{aligned} \tag{4}$$

with s running over all the lattice sites and δ over nearest neighbors only. In the spirit of the RSJ model, a dissipation term that takes into account the normal current junction resistance, and a noise term that brings the system to thermal equilibrium should be added to Eq. (4). The dissipation term is taken to have the form

$$-\eta\sum_\delta(\dot\theta_i-\dot\theta_{i+\delta})=-\eta\sum_{s,l}G_{is}^{-1}C_{sl}^{-1}p_s=-\sum_l\eta_{il}p_l\ . \tag{5}$$

Here, G_{ij} is the discrete Green function for the square lattice, $\eta=(\hbar/2e)^2/R$ with R the normal resistance of the junction and we define a dissipation matrix,

$$\eta_{ij}=\eta\sum_l G_{il}^{-1}C_{lj}^{-1}\ .$$

In conclusion, we have the following set of coupled Langevin equations:

$$\begin{aligned}&\dot\theta_i=\alpha\sum_s C_{is}^{-1}p_s\ ,\\ &\dot p_i=E_J\sum_\delta\sin(\theta_{i+\delta}-\theta_i-A_{i,i+\delta})-\sum_s\eta_{is}p_s+\lambda_i(t)\ ,\\ &\langle\lambda_i(t)\rangle=0\ \text{ and }\ \langle\lambda_i(t)\lambda_j(t')\rangle=2T\eta_i\delta(t-t')\ .\end{aligned} \tag{6}$$

Here, T is the temperature (in units of k_B) and the noise correlation is just the result of the classical fluctuation-dissipation theorem. Note that, because of the nonlocal character of the dissipation in Eq. (5), the thermal noise $\lambda(t)$ is spatially correlated.

Particular choices of the matrix C_{ij} may give complicated equations involving long-range interactions. This is the case, for instance, if we consider the capacitance between islands, C_1. Then we have $C_{ij}^{-1}=G_{ij}/C_1$, where $G_{ij}=G(i-j)$ behaves asymptotically like $\log(i-j)$. Although we have made preliminary investigations in this general case, we restrict ourselves here to a simpler situation in which the capacitance matrix is *diagonal*: $C_{ij}=C_0\delta_{ij}$. Such a choice is realistic for some kinds of array geometry in which only the capacitance between island and background is relevant.[13] For this case the normalized Langevin equation can be written as

$$\dot{\theta}_i=\bar{p}_i,\quad \dot{\bar{p}}_i=J\sum_{\delta}\sin(\theta_{i+\delta}-\theta_i-A_{i,i+\delta}) -\bar{\eta}\sum_{\delta}(\bar{p}_i-\bar{p}_{i+\delta})+\tilde{\lambda}_i(t)\ , \tag{7}$$

$$\langle\tilde{\lambda}_i(t)\rangle=0\ \text{ and }\ \langle\tilde{\lambda}_i(t),\tilde{\lambda}_j(t')\rangle=2\bar{\eta}G_{ij}^{-1}\tilde{T}\delta(t-t')\ .$$

Here $\bar{p}=p/\hbar$, the dimensionless parameters in these equations are $J=E_JC_0/\alpha$, $\bar{\eta}=\hbar/2e^2R$, $\tilde{T}=TC_0/\alpha$, and the time unit is $\tau=\hbar C_0/4e^2$. In these units the plasma frequency is $\omega_J^2=E_J\alpha/C_0\hbar^2$. It is straightforward to make contact between this dynamics and that proposed by Shenoy[2] and used in MD simulations by Mon and Teitel.[1] Our dynamics reduces to theirs in the overdamped limit ($\eta\to\infty$), and we have quantitatively reproduced the I-V characteristics of Ref. 1 for the $f=0$ and $\frac{1}{2}$ cases studied there. We will concentrate on this overdamped regime here. However, it is worthwhile to note that from a numerical point of view our equations have some advantages. Specifically, the computing time grows like L^2 and not L^4 as in Ref. 1, allowing the use of larger lattices. This is simply because by using a coupled set of differential equations we can avoid the inversion of the dissipation matrix $\eta_{ij}(\eta_{ij}^{-1}=G_{ij}/\eta)$. Finally, in order to simulate nonequilibrium dynamics a uniform external current I is injected along an edge of the array and removed at the opposite edge. This is achieved by adding to the Hamiltonian a term[14]

$$H_1=-J_1\sum_j(\theta_{i=1,j}-\theta_{i=Lx,j})\ , \tag{8}$$

where $J_1=(\hbar/2e)I$. This term creates a "washboard" potential in which a phase slip of 2π over a local minimum induces voltage difference as defined below [Eq. 9(a)]. Periodic and free boundary conditions in the y and x direction, respectively, were used.

We have integrated Eqs. (7) using a second-order Runge-Kutta algorithm for stochastic differential equations[15] with time steps of 0.05τ. The time-dependent voltage across the array, as well as its time average, were measured. The dimensionless voltage and its power spectrum are defined as

$$V(t)=\frac{\bar{\eta}}{L}\left[\sum_j(\bar{p}_{i=(1,j)}-\bar{p}_{i=(Lx,j)})\right] \tag{9a}$$

and

$$S(\omega)=\left|\int_{-\infty}^{+\infty}V(t)e^{i\omega t}dt\right|^2\ , \tag{9b}$$

respectively. Fourier transforms were calculated using a 4096-point fast Fourier transform algorithm and averaging over different initial times (typically 4) to reduce the standard deviation of fluctuations.

Phase and fractional charge configurations were displayed (see the figures), allowing us to follow the dynamics of individual vortices and domain walls. The fractional charge q is calculated as the circulation of the gauge invariant phase around a plaquette

$$q=\frac{1}{2\pi}\sum_{\text{plaquette}}(\theta_i-\theta_j-A_{ij})=m-f\ , \tag{10}$$

where $(\theta_i-\theta_j-A_{ij})$ is restricted to be in the interval $(-\pi,\pi)$. m takes the values 1 and 0 with density $\frac{1}{3}$ and $\frac{2}{3}$, respectively, giving charge neutrality. Using these charge variables, the system is equivalent to a Coulomb gas driven by a uniform electric field.[1,5,16]

Most of our simulations were made on 36×36 lattices in which finite size effects are expected to be small. Simulation in 16×16 lattices[1] show essentially unchanged behavior. The parameters used in the Eqs. (7) were $J=1$, $\bar{\eta}=5$ which gives excellent agreement with previous results for $f=0$ and $\frac{1}{2}$ at finite temperature.[1] With these parameters we are in the overdamped regime discussed in Ref. 2, i.e., $\omega_JRC\ll1$.

III. RESULTS AND DISCUSSION

A. $T=0$ simulations

In this section we report results for $f=\frac{1}{3}$ obtained with the model described in Sec. II. Simulations at temperature $T=0$, although not relevant for comparison with experimental results because of quantum effects, give a perspective on possible extended defects (domain walls), which are responsible for flux flow mechanisms.

The first effect of the inclusion of a magnetic field is a critical current reduction. Figure 1 shows the I-V curves for several values of parameter $f(0,\frac{1}{2},\frac{1}{3})$. For $f=0$, the array behaves like a single Josephson junction obeying the well-known characteristic $V\approx(I^2-I_c^2)^{1/2}$, where I_c is the critical current of a single junction. Using our parameters $I_c=1$. For $f=\frac{1}{2}$ and $\frac{1}{3}$, $I_c\approx0.35$ and 0.1375, respectively, and a more complex behavior is observed. It is very important to emphasize that the $T=0$ "depinning" at $I_c(f)$ is fundamentally different for $f=0$ and $f\neq0$. If $f=0$ the ground-state configuration is spatially uniform, and, in the absence of impurities, temperature, or an inhomogeneous driving field, the voltage response remains spatially homogeneous for $I>I_c(0)$. However, in the presence of a magnetic field ($f\neq0$), the ground state has spatial structure and becomes depinned at $I_c(f)$ via instabilities of finite wave-vector modes which saturate, in the nonlinearity of the pinning potential, as a wall-antiwall nucleation process. Thus, the I-V threshold characteristics for $f\neq0$ are quite different from $f=0$

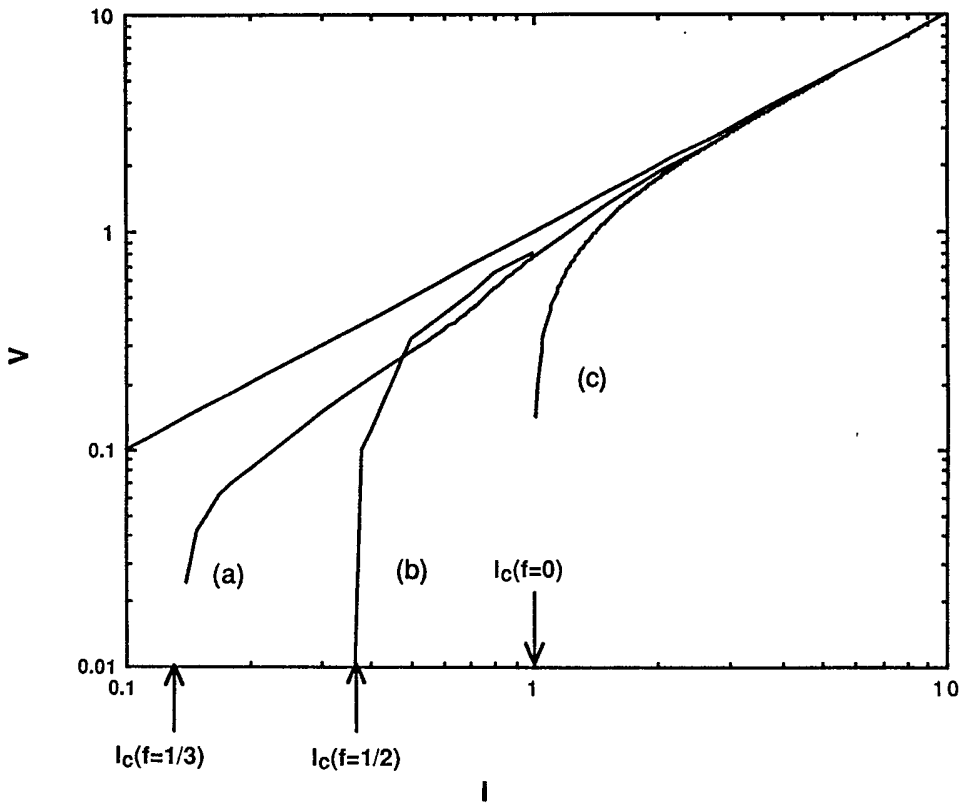

FIG. 1. *I-V* curves for different external magnetic fields: (a) $f=\frac{1}{3}$; (b) $f=\frac{1}{2}$ (data taken from Ref. 1; (c) $f=0$. Straight line is the ohmic limit. Arrows show the respective critical current values. Note the log-log scale.

(above). Only at $I \gg I_c(f)$ does the background flow easily as for $f=0$ with $I > I_c(0)$.

Figure 2 shows the $T=0$ *I-V* and *I-R* ($R=dV/dI$) curves for the case $f=\frac{1}{3}$, from which several interesting features can be noted. Four different regions can be clearly distinguished. First, A is a superconducting region ($I < I_c$, $I_c \approx 0.1375$) in which no voltage is generated and no flux flow can be observed. A second region, B,

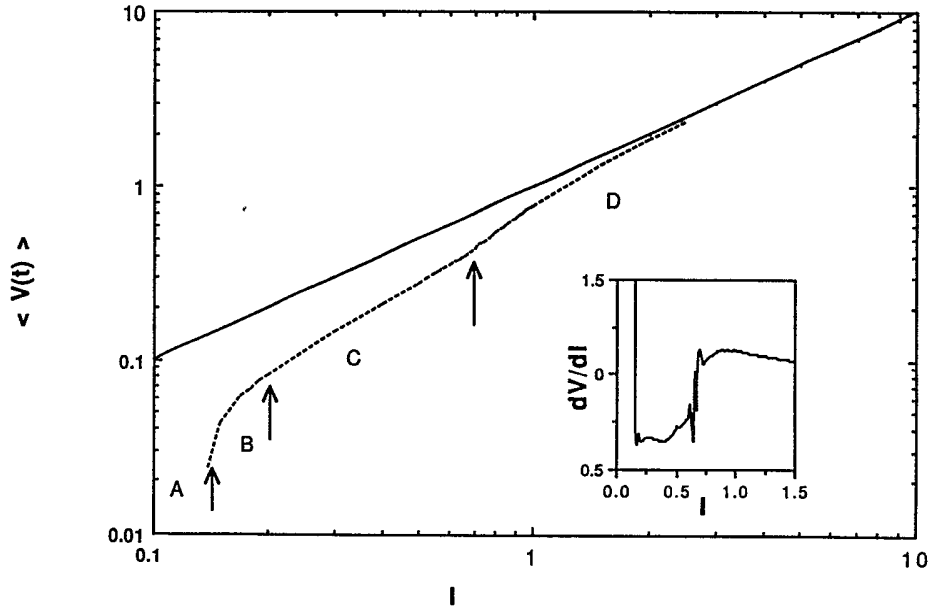

FIG. 2. *I-V* curve for $f=\frac{1}{3}$ at $T=0$ (dotted line). Solid straight line gives the ohmic limit. Arrows show separations between space-time regimes discussed in the text. Inset shows the *I-R* curve. Note the discontinuity at $I \approx 0.68$.

follows the onset of the nonzero voltage. Finally two regions, C and D, with near-linear characteristics separated by a sharp transition in the resistance. In each of the regions, different space-time dynamical behaviors have been observed. Discarding the pinned superconducting A phase, which is not of major interest for the present purposes, we review the other regions.

Region B ($I_c < I < 0.2$). This rich phase presents a broad spectrum of frequencies. Figure 3 shows the time dependence and power spectrum of the voltage for two different values of I near the boundaries with regions A and B. For higher currents a broad spectrum appears although some frequencies can be distinguished. As I_c is approached, the spectrum becomes noisier and more "chaotic" or "intermittent." In the following we relate this behavior with the domain-wall textures.

Regions C ($0.2 < I < 0.68$) *and D* ($I > 0.68$). In these parts of the I-V curve the dynamics is dominated by the ac Josephson effect. However, many properties (critical currents, the shape of the I-V curve, etc., show deviations from single junction behavior: cooperative interactions (i.e., many junction) effects are evidently involved. As shown in Fig. 4 the response is highly anharmonic for low currents as I_c is approached from above. The C and D regions are separated by a distinct change in the slope of the I-V curve (see inset of Fig. 2).

In order to understand these behaviors we have followed the dynamics of the flux lattice, relating different defect patterns to the various dynamical behaviors. We initialized all of our simulations in the ground state for $I = 0$.[3,5] Figure 5 shows configurations of the flux lattice in the regions of interest. For $I < I_c$ the flux lattice is pinned by the lattice descreteness and no voltage is developed [Fig. 5(a)]. For $I > I_c$ the ground state is modulationally unstable and domain walls are nucleated. Their density increases as I increases and for a high enough density of domain walls ($I > 0.2$) ordered superlattices of walls are formed [Figs. 5(c) and 5(d) are good examples]. However, a uniform motion of these superlattices cannot give an ac effect. (This is similar to the overdamped behavior of the sine-Gordon chain where only an inhomogeneous driving field produces an ac oscillations[17].) The motion is driven by injection of linear defects (domain wall in the lattice of domain walls) through

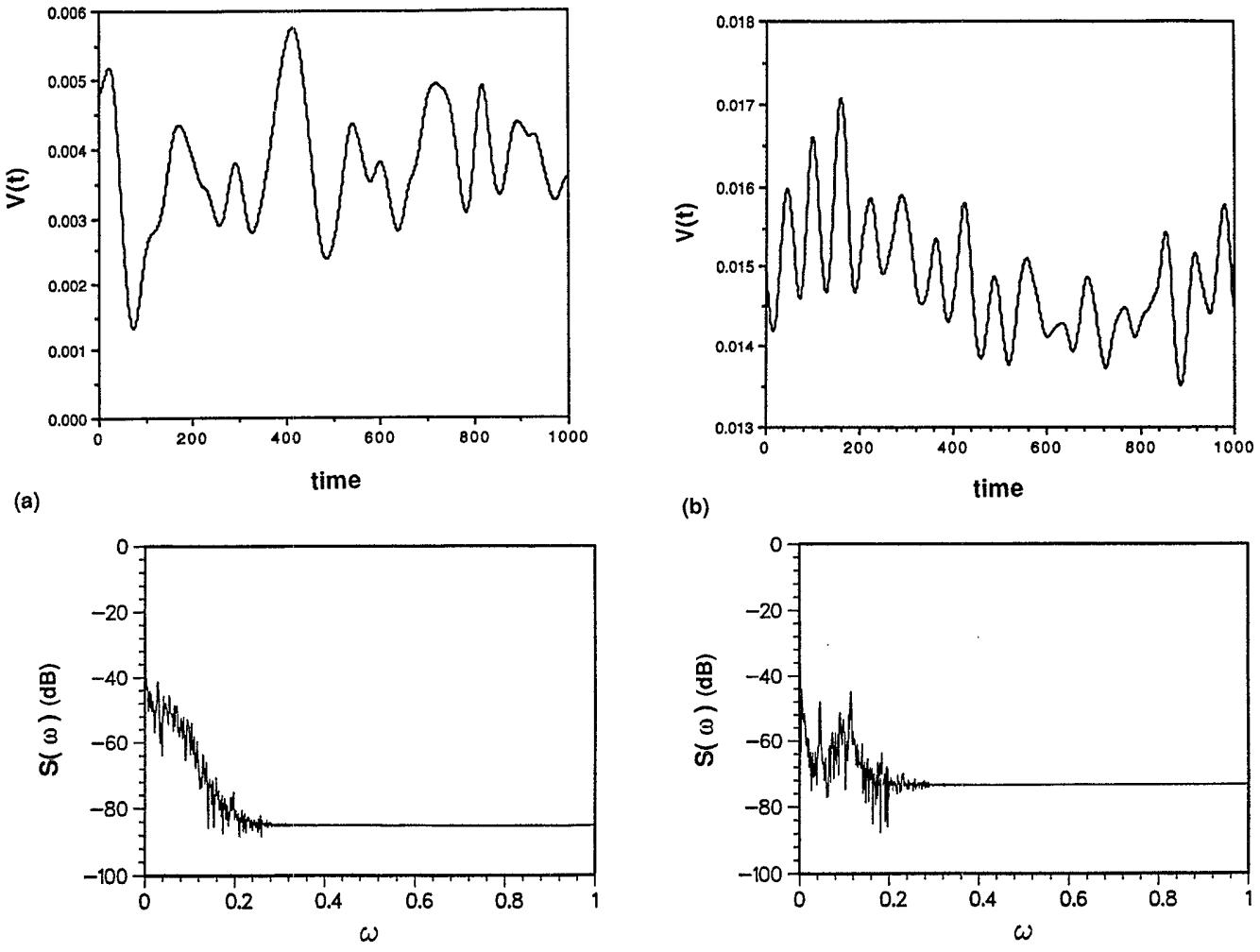

FIG. 3. (a) Time dependence and power spectrum of the voltage drop across the array [Eqs. 9(a) and 9(b)] for $I = 0.14$. (b) Same as (a) for $I = 0.19$.

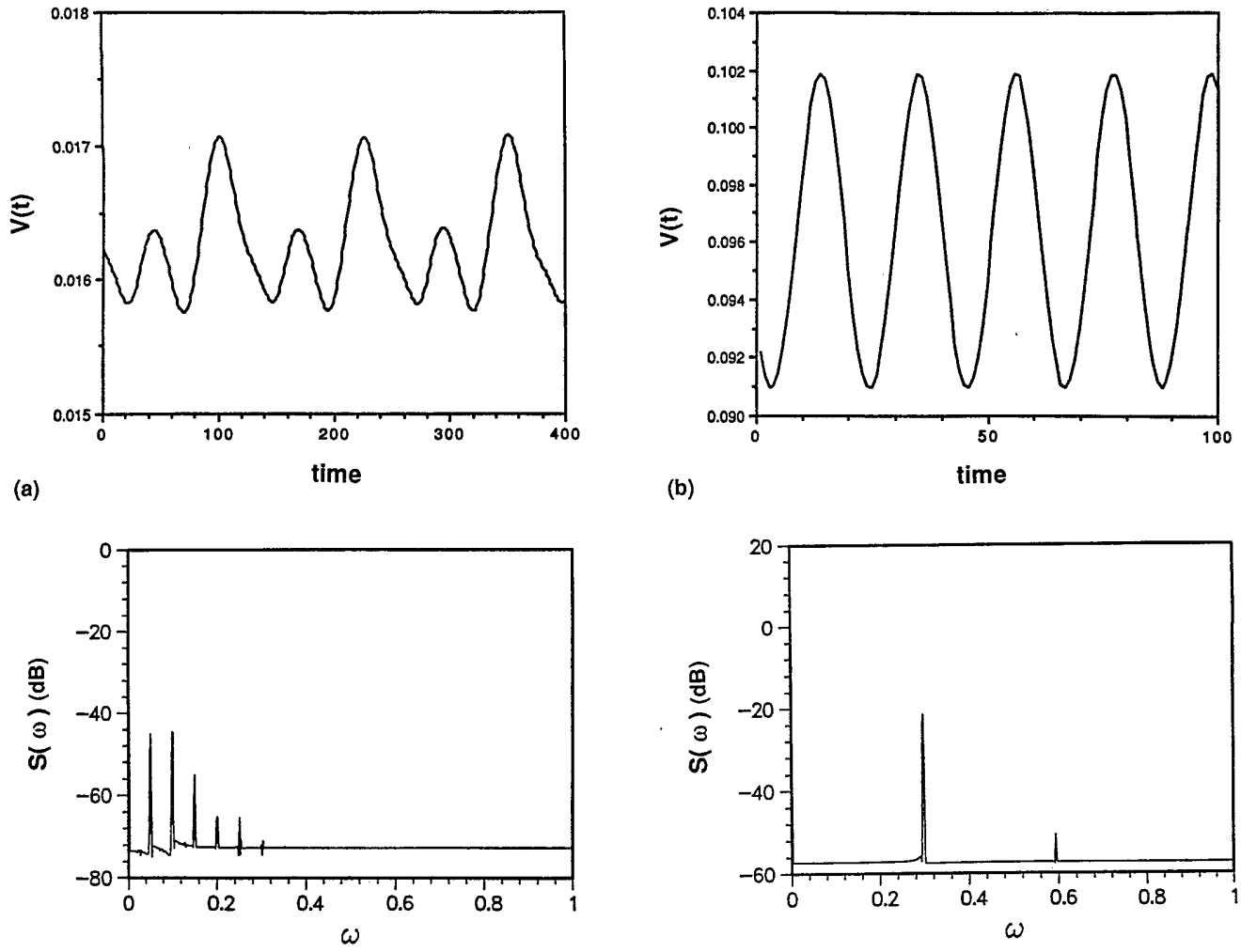

FIG. 4. (a) Same as Fig. 3 for $I=0.2$. (b) Same as Fig. 3 for $I=0.74$.

the open boundaries, which annihilate inside the lattice. For higher fields ($I\approx 0.6$) a uniform pattern of domain walls is found [Fig. 5(e)]. This pattern is unstable at $I_{c1}\approx 0.68$ and melts into another pattern [Fig. 5(f)] via nucleation of a new defect type—composed of a mixture of ground-state-like configuration [see Fig. 5(f)].[18] Now the mechanism for dynamics is repeated. The formation of the regular domain-wall lattice can be understood by assuming a repulsive interaction between them, as in Frenkel-Kontorova models.[19] An interesting feature is the ratio $\langle V(t)\rangle/\omega\approx\frac{1}{3}$ over the whole range in which the frequency is well defined. This means that for each cycle the whole flux lattice moves by one unit of flux due to overall motion of the domain-wall lattice. As the density of extra positive charges ($m=1$) is $\frac{1}{3}$, the preceding ratio is constant.

In region B (low density of domain walls) an aperiodic lattice of walls appears. At low density the field-nucleated domain walls are nearly pinned by the periodic potential forming spatially irregular moving lattices .[19,20] Each domain wall is dominated by the local potential created by its individual environment, rather than the interaction with neighboring walls which leads to the periodic superlattices in region C. The multiplicity of environments in the nonperiodic lattice leads to a multifrequency regime, as in driven Frenkel-Kontorova models.[20] Thus this scenario can be understood as the transition from a pinned commensurate phase (the $I<I_c$ superconducting phase) to a dynamic incommensurate one—a "chaotic" lattice of pinned domain walls. In this way, the competing interactions lead to an explicit connection between "noisy" dynamics and spatial structure.

It should be noted that, due to the transverse rigidity of the domain walls at $T=0$, we can discuss them using a close analogy with the dynamics of discrete one-dimensional models, e.g., 1D Frenkel-Kontorova. This analogy breaks down, however, at finite temperature where inhomogeneities can play the important role of nucleating transverse dynamics.[21] We now discuss $T>0$ results.

B. $T\neq 0$ simulations

At finite temperature two kinds of simulations have been made. First, $I=0$ simulations (with periodic bound-

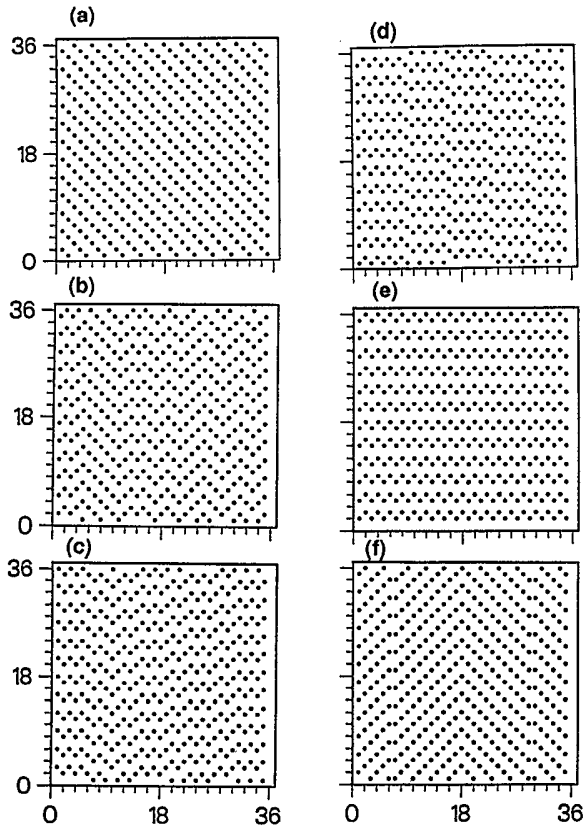

FIG. 5. Flux lattice configuration at $T=0$ for (a) $I<I_c$ (ground state for $f=\frac{1}{3}$); (b) $I=0.14$ (region B); (c) $I=0.2$ (region C); (d) $I=0.3$ (region C); (e) $I=0.6$ (region C); (f) $I=0.8$ (region D). Dots signify $m=1$, i.e., $q=\frac{2}{3}$.

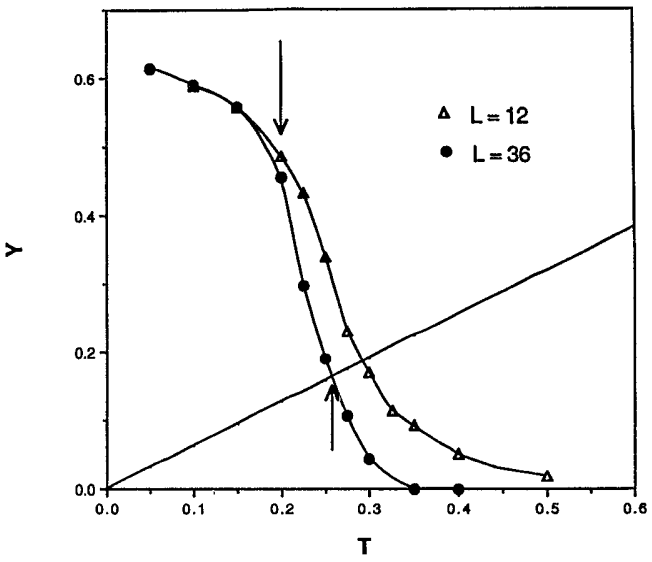

FIG. 6. Helicity modulus (Y) for 12×12 and 36×36 lattices. Continuous line, $Y=2\pi/T$, shows the expected magnitude of the universal jump according to the Kosterlitz-Thouless theory. Arrows show the "transition" temperatures cited in the text.

ary conditions in both directions) in order to calculate thermodynamics properties and locate the phase transition to the normal (i.e., nonsuperconducting) state. The nature of the corresponding phase transition in the frustrated XY models is interesting because it shares characteristics of both XY and Ising models.[5,12] The helicity modulus (HM) has been used as an indicator of the phase transition[5,22] based on the fact that a universal jump is expected[23] at T_c. Although there is clear evidence that this is true for the neutral Coulomb gas ($f=0$), a higher jump is seen in the frustrated case.[5,22] Figure 6 shows the simulation of HM for two different lattice sizes (other intermediate values have been used). Using the universal jump criterion implies $T_c\approx0.275$. However, the jump is visibly larger, and in fact domain walls begin to appear at $T\approx0.2$. This estimation of $T_c\approx0.2$ is in excellent agreement with the result for the two-dimensional *charged* Coulomb gas.[22] We have not attempted further measurements that might distinguish unambiguously between a single or two transitions (KT like and Ising like). However, it seems very likely that these temperature must be differentiated. For example, in Fig. 7 we show equilibrium configuration for $T=0.2$ and 0.3. It is clear that for $T=0.2$ domain-wall excitations are responsible for the decreasing of the HM and vortex-antivortex pairs do not appear. This situation persists in the intermediate temperature region ($0.2<T<0.275$). At $T>0.275$ an isotropic liquidlike state is observed due to the proliferation of vortexlike excitations. This scenario would be consistent with two transitions, the first of Ising character yielding a non-XY decrease of HM. Once the HM

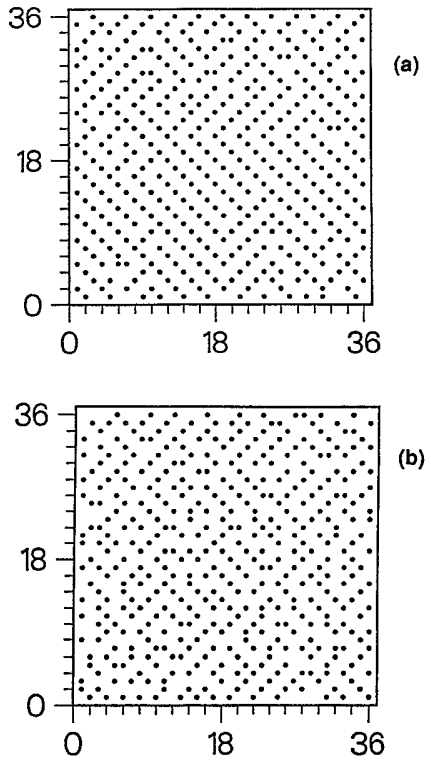

FIG. 7. Equilibrium flux lattice configuration for (a) $T=0.2$ and (b) $T=0.3$.

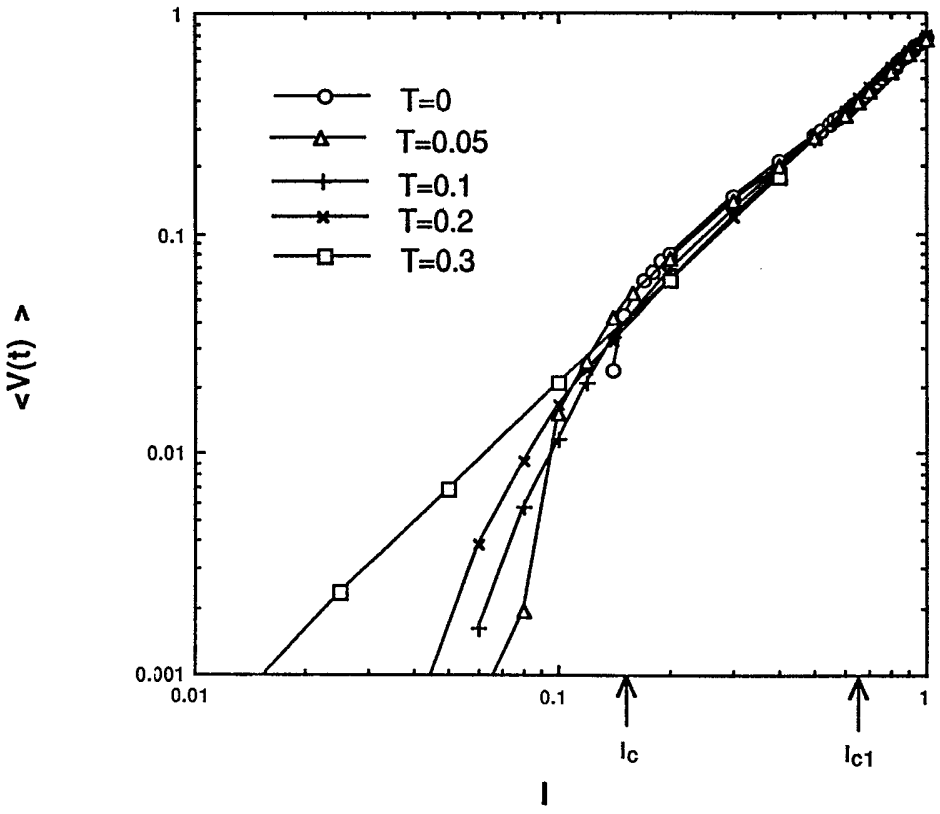

FIG. 8. *I-V* curve at finite temperatures.

reaches the critical value of $(2\pi/T)$, unbound vortex-antivortex pairs can develop and the domain-wall structure melts to a disordered phase.

Next we study the *I-V* characteristics at finite temperature. Figure 8 shows *I-V* curves for several different temperatures. As can be anticipated, the $T=0$ critical current is smoothed due to the thermally excited vortex-antivortex pairs and domain walls, and an excess voltage appears below I_c ($T=0$). This region should show a characteristic power-law behavior if Kosterlitz-Thouless (*XY*) theory prevails. However, we have been unable to fit the data to such a form. As also pointed out by Mon and Teitel[1] this can be interpreted as the influence of the domain walls on the dynamics. In fact, a finite density of walls can be observed at low currents and temperatures. At $I \approx I_c$ the curves cross, *decreasing* the voltage with increasing temperature. In the region *C*, near the ohmic limit all curves converge—only a very slight increase of voltage with temperature is observed. It is interesting also to observe the *I-R* curve (Fig. 9) where one can appreciate the broadening of the transition at I_{c1}. At $T=0.2$ only a smooth curve is obtained giving further evidence of a phase transition or strong crossover at this temperature.

We can understand the preceding behavior by identifying the mechanism for domain-wall motion more precisely. Below the $T=0$ critical current, a rigid domain wall cannot overcome the pinning potential. However, due to thermal fluctuations, a domain wall can lose its rigidity by nucleation of kink-antikink structures which propagate on the walls *transversely* to the domain-wall motion. We can identify the instabilities which saturate into kink-antikink pairs as thermally excited vortex-antivortex pairs which unbind in opposite directions (along the *y* axis) driven by the electric field associated

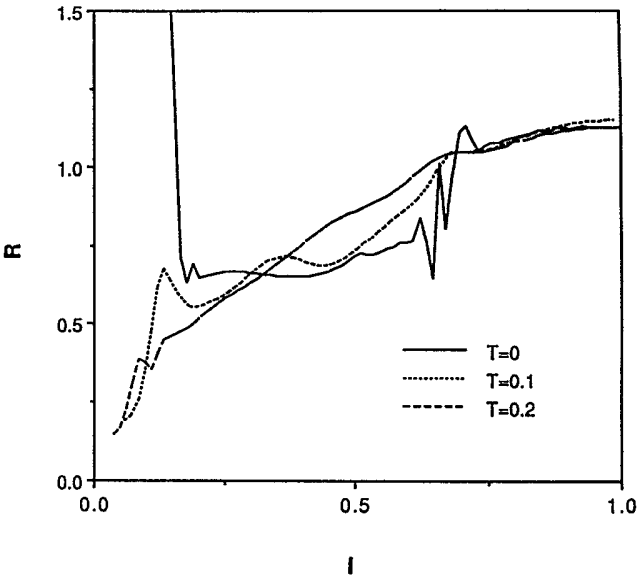

FIG. 9. *I-R* curve at finite temperatures.

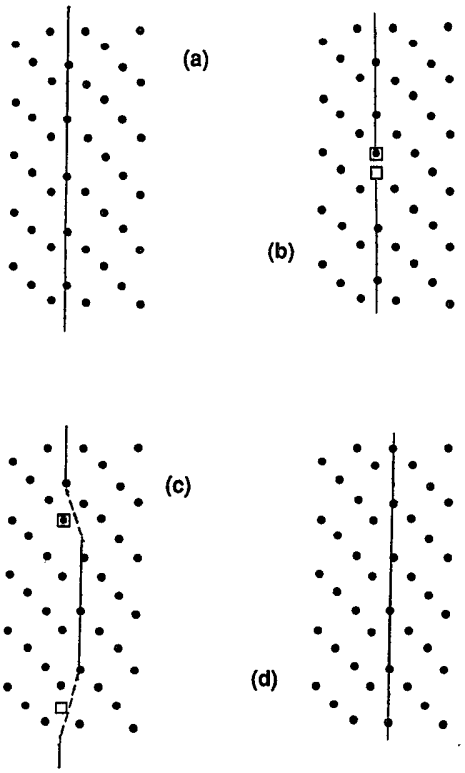

FIG. 10. Mechanism for domain motion at low currents and finite temperature: (a) domain-wall structure; (b) vortex-antivortex (kink-antikink) pair created on the wall; (c) transversal pair separation giving longitudinal motion of the domain wall; (d) final configuration following annihilation of the pair through the periodic boundary condition. Domain wall and vortices are indicated to guide the eye. Note that this pair nucleation occurs randomly on each domain wall and that several nucleation events can appear on the same wall.

with the external current. This mechanism is easily observed in simulations at low current and low temperature in which the density of both is small. Figure 10 illustrates the motion of a domain wall by this transverse instability. First, a vortex-antivortex pair relative to the rigid domain wall is created. (In the charged Coulomb gas language this excitation corresponds to an interstitial charge hole in the lattice.) Then this pair separate to opposite boundaries in the y direction. Due to the periodic boundary conditions in this direction, they annihilate. More complicated situations have been observed when several pairs are randomly nucleated on the same domain wall. An important consequence of this interaction mechanism between vortex and domain-wall structures is the roughening of the domain-wall lattice. At low currents this roughening only has the effect of facilitating the domain-wall motion but does not influence the interaction between walls since the wall width is much smaller than the wall separation. Thus, the thermal enhancement of the voltage below I_c is understood by the motion of domain walls via transverse instabilities. It is likely that extrinsic inhomogeneities could act as similar nucleation sites for such transverse wall instabilities.

Close to I_c (where even the $T=0$ dynamics is noisy) the flux lattice patterns become more complicated and there is little regularity in the dynamics. For these currents (see Fig. 8), domains walls are induced both by thermal fluctuations and by the current. Their current-induced density rapidly increases and dominates, and the transverse wall roughening leads to non-negligible domain-wall–domain-wall interaction and entanglement. Both mechanism of motion (rigid wall flow and transverse-instability-assisted flow) compete giving a rapid increase of voltage (from the increased density of depinned domain walls) at $I > I_c$ but a decrease of voltage with *increasing* temperature (from the increased vortex-antivortex density decorating the walls).

At even higher currents ($I > I_{c1}$), the field driven texture transforms to a new pattern (as for $T=0$) and there is very little T dependence (see Fig. 8). Here, the domain wall and vortex-antivortex excitations are primarily field-nucleated (the only role of the temperature is to create the inhomogeneity necessary for local vortex-antivortex nucleation). Again, an entangled structure of domain walls [of the type shown in Fig. 5(g)] is observed but their motion is dominated by a uniform sliding in the strong external field, giving little T dependence.

Finally, we note that, except at low currents ($I < I_c$), the $T=0.2$ and $T=0.3$ curves coincide. This suggest that internal wall structure is not relevant to the conduction processes at these high temperatures. The high density of domain wall and vortex excitations (thermally or current excited) give similar textures in the flux lattice structure at both temperatures, and the dynamics is again primarily a rigid sliding of the texture.

IV. CONCLUSIONS

In this study we have used a Langevin molecular-dynamics simulation to examine the flux lattice *dynamics* in the superconducting phase of an array of Josephson junctions in an external perpendicular magnetic field. We have been able to correlate the response of an external dc driving current with the diverse spatial configurations of the flux lattice. Because of the inhomogeneous ground state and the underlying XY symmetry, several regimes occur. These are summarized schematically in Fig. 11 and include the following.

(i) At *zero temperature,* the flux lattice behaves like an effective 1D model of interacting domain walls in a periodic potential. Different regimes in the I-V curves (Sec. III A) can be understood in this way. The dynamical properties are controlled by the defects nucleated with respect to the ordered flux lattice. These defects (domain walls) arrange in ordered or "chaotic" lattices (due to the lattice discreteness) giving the various dynamical behaviors described in Sec. III.

(ii) At *finite temperatures* the appearance of transverse instabilities breaks the equivalence with 1D models. These instabilities have been assigned to vortex-antivortex excitations moving transversely to the domain-wall motion. Then, the motion of the domain wall is driven by these local defects leading to a finite voltage even for $I < I_c$. In our simulations, inhomo-

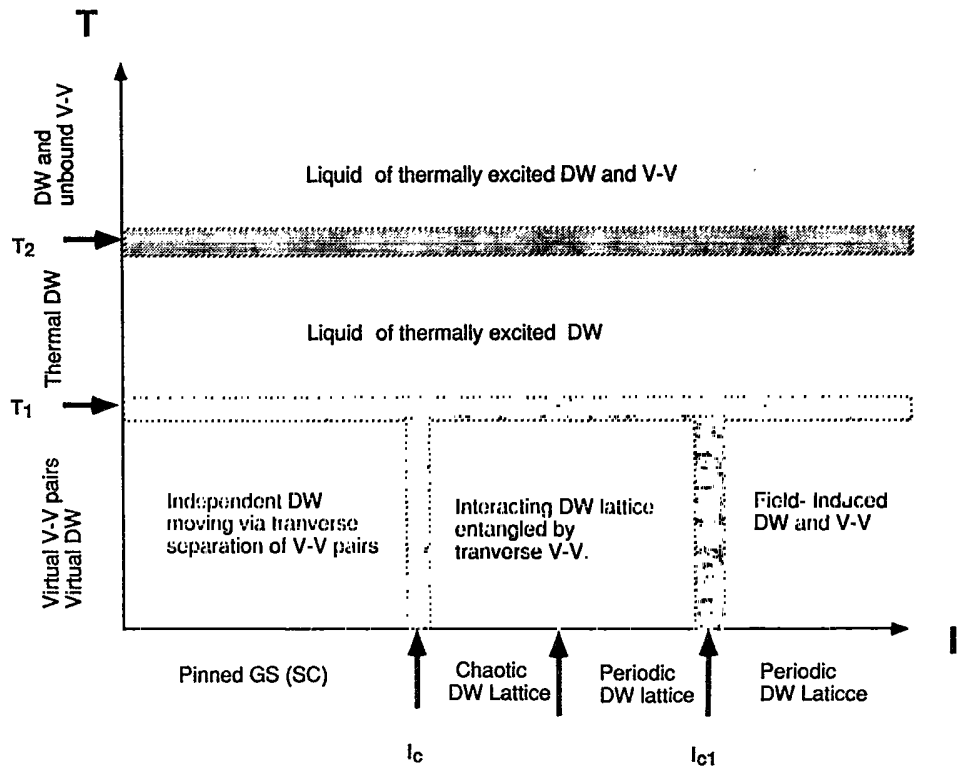

FIG. 11. Proposed T-I phase diagram (schematic). Boundaries are diffuse except along $T=0$ and $I=0$. Notation: DW and V-V stand for domain wall and vortex-antivortex pair, respectively.

geneities are induced by thermal noise although impurities could also nucleate them[21]—such an effect has been observed in a JJA with missing bonds also giving a lowering of the critical current.[6]

We have observed a response regime B with multifrequency (possibly including chaotic) dynamics. In view of the space-time relationships established in this paper, we suggest that *noise* measurements may be a useful experimental diagnosis for textures in dynamic vortex lattices. A similar suggestion is appropriate to other systems with pinned incommensurate ground states which can be depinned by an external driving force—e.g., pinned-charge-density waves,[24] a superconducting layer in an external magnetic film with vortex lattice pinning from modulation of the film thickness,[7] or even layered high-temperature superconductors. It is particularly important to appreciate the various interactions between field-induced and thermally induced vortex and domain-wall patterns that our results have illustrated. We have seen that these interactions can both enhance and inhibit flux flow. Modeling wall-vortex interaction in the presence of a driving field is an important theoretical challenge. One possible direction is to map the coupled set of Langevin equations [Eq. (7)] to a Hamiltonian system in one higher spatial dimension. This is possible[25] in the overdamped limit considered here, for which a Lyapunov free energy can be identified. Then, the long-time attractors and excited states will correspond to ground and metastable states in this effective higher dimensional, competing length scale Hamiltonian.

Our future work will address the effects of disorder in these systems. As we already argued impurities can be expected to influence the dynamical properties, e.g., critical currents. This may be especially important in superconductors. There are many ways to introduce disorder in a JJA. Positional disorder has been studied recently,[26] attempting to explain the glassy behavior of high-T_c superconductors. Other source of disorder could be the existence of Josephson junctions on different length scales. Also finite scale dynamical properties (e.g., frequency-dependent impedance or conductivity) are important in JJA's and real superconductors[7] and will have their own characteristic signatures of glassy situations. In general, we can expect an important future for dynamical studies of JJA's—both as an experimentally controlled environment for probing glassy dynamics in competing interaction systems and as a model for vortex flow phenomenology in real superconductors.

ACKNOWLEDGMENTS

We are grateful for valuable discussions and correspondence with H. Beck, A. P. Kampf, P. Martinoli, and S. Shenoy. One of us (F.F.) acknowledges the Spanish Ministry of Education and Science for support. Work at Los Alamos was supported by the U.S. Department of Energy and the Center for Materials Science.

*Permanent address: Departamento de Ciencia y Tecnología de Materiales y Fluídos and Instituto de Ciencia de Materiales de Aragón, Universidad de Zaragoza-C.S.I.C., 50009 Zaragoza, Spain.

[1]K. K. Mon and S. Teitel, Phys. Rev. Lett. **62**, 673 (1989).

[2]S. R. Shenoy, J. Phys. C **18**, 5163 (1985); R. Mehrotra and S. R. Shenoy, Europhys. Lett. **9**, 11 (1989).

[3]T. C. Halsey, Phys. Rev. B **31**, 5728 (1985).

[4]T. C. Halsey, Phys. Rev. Lett. **55**, 1018 (1985).

[5]S. Teitel and C. Jayaprakash, Phys. Rev. B **27**, 598 (1985); Phys. Rev. Lett. **51**, 1999 (1983).

[6]W. Xia and P. L. Leath, Phys. Rev. Lett. **63**, 1428 (1989).

[7](a) P. Martinoli, H. Beck, M. Nsabimana, and G. A. Racine, in *Percolation, Localization and Superconductivity,* edited by A. L. Goldman and S. A. Wolf (Plenum, New York, 1984); (b) Ch. Leeman, Ph. Lerch, G.-A. Racine, and P. Martinoli, Phys. Rev. Lett. **56**, 1291 (1986).

[8]M. Tinkham and C. J. Lobb, Solid State Phys. **42**, 91 (1989).

[9]J. M. Kosterlitz and D. J. Thouless, J. Phys. C **6**, 1181 (1973); J. M. Kosterlitz, *ibid.* **7**, 1046 (1974); J. V. José, L. P. Kadanoff, S. Kirkpatrick, and D. R. Nelson, Phys. Rev. B **16**, 1217 (1979).

[10]V. Ambegaokar, B. I. Halperin, D. R. Nelson, and E. D. Siggia, Phys. Rev. **21**, 1806 (1980); B. I. Halperin and D. R. Nelson, J. Low. Temp. Phys. **36**, 599 (1979).

[11]See articles in *Competing Interactions and Microstructures: Statics and Dynamics,* edited by R. LeSar, A. R. Bishop, and R. Heffner, Vol. 27 of *Springer Proceedings in Physics Series* (Springer-Verlag, Berlin, 1988).

[12]M. Yosefin and E. Domany, Phys. Rev. B **32**, 1778 (1985); E. Granato and J. M. Kosterlitz, *ibid.* **33**, 4767 (1986).

[13]R. M. Bradley and S. Doniach, Phys. Rev. B **30**, 1138 (1984). These authors discuss similar *quantum* models in 1D chains.

[14]V. Ambegaokar and B. I. Halperin, Phys. Rev. Lett. **22**, 1364 (1969).

[15]H. S. Greenside and E. Helfand, Bell Syst. Tech. J. **60**, 1927 (1981). It is easy to prove that second-order algorithm reported in this reference can be extended to spatially correlated noise.

[16]For a review of the 2D Coulomb gas, see P. Minnhagen, in *Percolation, Localization and Superconductivity,* edited by A. L. Goldman and S. A. Wolf (Plenum, New York, 1984).

[17]A. R. Bishop, B. Horovitz, and P. S. Lomdahl, Phys. Rev. B **37**, 4853 (1988).

[18]Note in the Fig. 5(f) that the new pattern is symmetric respect the $L/2$ line. This is a consequence of the initial conditions. On this line domain walls coming from the edges annihilate.

[19]S. Aubry, Festkörperprobleme XXV, 85 (1985); P. Bak, Rep. Prog. Phys. **45**, 587 (1982).

[20]S. Aubry, Physica D 7, 240 (1983).

[21]J. Pouget, S. Aubry, A. R. Bishop, and P. S. Lomdahl, Phys. Rev. B **39**, 9500 (1989); J. C. Ariyasu and A. R. Bishop, *ibid.* **35**, 3207 (1987).

[22]G. S. Grest, Phys. Rev. B **39**, 9267 (1989).

[23]D. R. Nelson and J. M. Kosterlitz, Phys. Rev. Lett. **39**, 1201 (1977).

[24]See articles by D. S. Fisher and G. Gruner, in Ref. 11.

[25]R. Eykholt, A. R. Bishop, P. S. Lomdhal, and E. Domany, Physica D **23**, 102 (1986).

[26]See, for example, W. Y. Shih, C. Ebner, and D. Stroud, Phys. Rev. B **30**, 134 (1984); I. Morgenstern, K. A. Müller, and J. G. Bednorz, Z. Phys. **69**, 33 (1987); E. Granato and J. M. Kosterlitz, Phys. Rev. Lett. **62**, 823 (1989); J. Choi and J. V. José, *ibid.* **62**, 320 (1989).